frontiers in Nanotechnology

ORIGINAL RESEARCH
published: 15 March 2021
doi: 10.3389/fnano.2021.627387

First-Principles Study on Optic-Electronic Properties of Charge-Ordered Indium Halide Perovskite $Cs_2In(I)In(III)Cl_6$ at High Pressure

*Yajing Wang[1], Shunwei Yao[1], Xiaolin Liu[1], Guohong Chen[2] and Lin Peng[1]**

[1]Department of Physics, Shanghai University of Electric Power, Shanghai, China, [2]Department of Physics, Shanghai Dianji University, Shanghai, China

Using the first principle method we studied, theoretically and in detail, the structural, optical, and electronic properties of a charge-ordered indium halide perovskite $Cs_2In(I)In(III)Cl_6$ at high pressure. In this structure, In1, In2, and In3 are octahedrally coordinated, whereas In4 is at the center of a pentagonal bipyramid. The charge of In on In1 and In2 sites can be assigned to 3^+, while In^+ occupies In3 and In4 sites. The results indicated that the band gap decreases, and the electron excitation produces the red-shift of peak value of optical absorption coefficient in visible and infrared regions with increasing pressure, and the reflectivity decreases in visible and infrared regions with increasing pressure. These theoretical results provide a basis for designing related inorganic halide perovskites.

Keywords: halide perovskites, band structure, charge-ordered indium, optic-electronic properties, high pressure

OPEN ACCESS

Edited by:
Yi Yu,
ShanghaiTech University, China

Reviewed by:
Xun Zhangxun,
ShanghaiTech University, China
Zhenzhu Li,
Imperial College London, United Kingdom

****Correspondence:***
Lin Peng
plpeng@shiep.edu.cn

Specialty section:
This article was submitted to Nanocatalysis, a section of the journal Frontiers in Nanotechnology

Received: *09 November 2020*
Accepted: *01 February 2021*
Published: *15 March 2021*

Citation:
Wang Y, Yao S, Liu X, Chen G and Peng L (2021) First-Principles Study on Optic-Electronic Properties of Charge-Ordered Indium Halide Perovskite $Cs_2In(I)In(III)Cl_6$ at High Pressure. Front. Nanotechnol. 3:627387. doi: 10.3389/fnano.2021.627387

INTRODUCTION

Halide perovskites with various compositions, dimensionalities, and morphologies, have been greatly developed over the last decade. The class of materials have a wide range of potential applications, such as photovoltaics, light-emitting diodes, photodetectors, and lasers, due to their remarkable optoelectronic properties (Dreizler and Gross, 1990; Retuerto et al., 2013; Yin and Kotliar, 2013; Filip et al., 2014; Amgar et al., 2016; He et al., 2017; Kovalenko et al., 2017; Vargas et al., 2017; Volonakis et al., 2017; Zhao et al., 2017; Han et al., 2018; Jeong et al., 2018; Lin et al., 2018; Lin et al., 2019a; Lin et al., 2019b; Tan et al., 2019; Chen et al., 2020; Li et al., 2020). Halide perovskites have the general formula ABX_3 (Lin et al., 2019a), and the crystal symmetry and phase stability can be determined using the Goldschmidt's tolerance factor t (Zhao et al., 2017). In the perovskite structure, a site can be occupied by either an inorganic ion (e.g., Cs^+, Rb^+, K^+) or an organic ion [e.g., $CH_3NH_3^+$ (MA^+), $HC(NH_2)_2^+$ (FA^+)]; B is a divalent metal cation (e.g., Pb^{2+}, Sn^{2+}, or Ge^{2+}) and X is a halide anion (e.g., I^-, Br^-, Cl^-). The B cation has six nearest-neighbored anions X, and the A cation occupies a vacancy formed by eight corner-sharing $[BX_6]^{4-}$ octahedrons (Lin et al., 2019a). Among the perovskite-type structure materials, the charge ordered materials $Cs_2B^+B^{3+}X_6$, such as $Cs_2Au^+Au^{3+}X_6$, and $Cs_2Tl^+Tl^{3+}X_6$ (X = Cl, Br, I), show unique properties, including potential high-T_c superconducting behaviors and semiconductor-metal transition at high pressures (Yin and Kotliar, 2013; Lin et al., 2019). For example, $Cs_2Tl^+Tl^{3+}Cl_6$ and $Cs_2Tl^+Tl^{3+}F_6$ perovskites were theoretically predicted to be potential superconductors if they were optimally doped and indicated high-T_c ~20 and ~30 K superconductivity under reasonably high pressures (Yin and Kotliar, 2013).

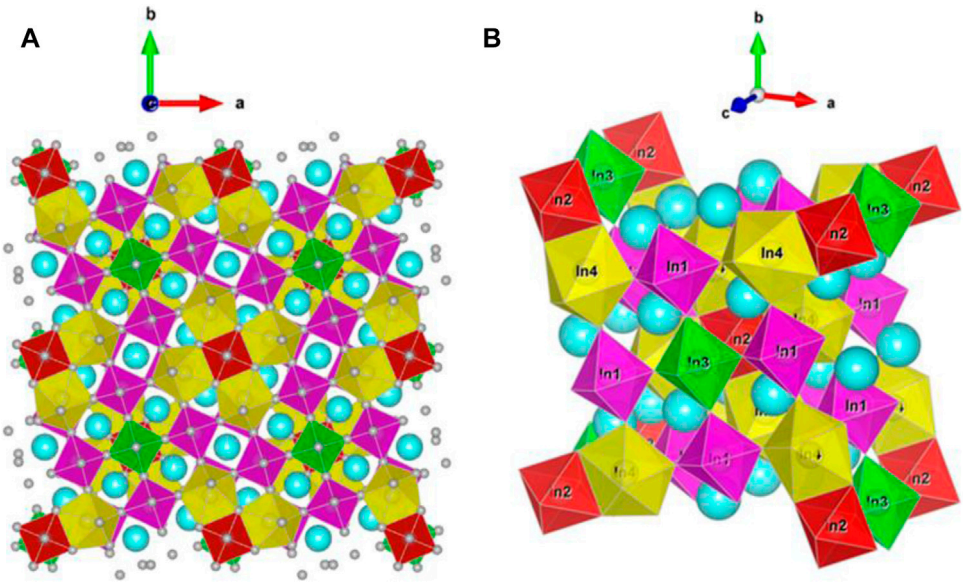

FIGURE 1 | (Color online) Crystal structure of Cs_2In**(I)**$In(III)Cl_6$ with the space group I4/m **(A)** super cell (2 × 2 × 2), **(B)** conventional unit cell. Color code: In1 = magenta, In2 = red, In3 = green, In4 = orange, Cs = blue, and Cl = gray.

TABLE 1 | Crystallographic data of $CsInCl_3$, according to the structural model described in the text [Fractional Atomic Coordinates (× 10^4)].

Compound	$CsInCl_3$			
Chemical formula, Mol. Wt.	$CsInCl_3$, 353.6			
Lattice dimensions, unit cell volume	$a = b = 17.1098(1)$ Å, $c = 11.0523(1)$ Å $\alpha = \beta = \gamma = 90^{\circ}$. 3,235.50(5) Å^3			
Space group	*I4/m*, #87			
Atom	*x*	*y*	*z*	Occupancy
Cs1	10,000	5,000	7,500	1
Cs2	6,099(3)	7,140(7)	7,661(7)	1
In1	8,007.6(8)	5,949.6(8)	10,000	1
In2	5,000	5,000	5,000	1
In3	5,000	5,000	10,000	1
In4	10,843(4)	7,439(3)	10,000	1
Cl1	8,474(4)	4,570(4)	10,000	1
Cl2	6,633(4)	5,488(5)	10,000	1
Cl3	7,539(4)	7,332(4)	10,000	1
Cl4	9,393(4)	6,396(5)	10,000	1
Cl5	7,992(3)	5,946(3)	7,708(6)	1
Cl6	5,000	5,000	7,269(8)	1
Cl7	5,671(5)	6,295(4)	5,000	1

These two compounds, together with a complete characterization of the samples were synthesized (Retuerto et al., 2013). $Cs_2Tl^+Tl^{3+}Cl_6$ is obtained as orange crystals in two different polymorphs: a tetragonal (I4/m) and a cubic (Fm-3m) phase. $Cs_2Tl^+Tl^{3+}F_6$ is formed as a light brown powder, also as a double cubic perovskite (Fm-3m). In all three $Cs_2Tl^+Tl^{3+}X_6$ phases, Tl^+ and Tl^{3+} were located in two different crystallographic positions that accommodate their different bond lengths. Recently, polycrystalline samples of $Cs_{1.17}In_{0.81}Cl_3$ were prepared by annealing a mixture of CsCl, InCl, and $InCl_3$, stoichiometric for the targeted $CsInCl_3$ (Tan et al., 2019). The composition $Cs_{1.17}In_{0.81}Cl_3$ with both corner-sharing and edge-sharing $InCl_6$ octahedra and $InCl_7$ pentagonal bipyramids, is isostructural with tetragonal $Cs_2Tl^+Tl^{3+}Cl_6$ (I4/m). Subsequently, the In^+/In^{3+}-based charge-ordered halide perovskite compound $Cs_2In^+In^{3+}Cl_6$ [$Cs_2In(I)In(III)Cl_6$] has also been successfully synthesized through a solid-state reaction method, which shows a semiconductor-to-metal phase transition under high pressures (Lin et al., 2019a).

Despite the tremendous progress which has been made, challenges still remain with perovskites, which call for a better understanding of the fundamental mechanisms of halide. Pressure, a thermodynamic variable, provides a powerful tool to tune structures and properties (Li et al., 2020). On one hand, in combination with *in situ* characterization methods, high-pressure research could experimentally provide a better fundamental understanding. On the other hand, the properties of materials could be theoretically predicated at high pressure. In this work we shall discuss, theoretically and in detail, the structural, optical, and electronic properties of $Cs_2In(I)In(III)Cl_6$ at high pressure.

COMPUTATIONAL METHODS

In this study, all structure optimizations are calculated by the generalized gradient approximation (GGA) with density functional theory (DFT) (Dreizler and Gross, 1990). The Perdew–Burke–Ernzerhof (PBE) functional is applied to describe the electron exchange correlation. At the present calculations, energy cutoff of plane-wave was set to be ^{400} eV, the special points sampling integration over the Brillouin zone were performed using a k-mesh of dimensions 4×4×4 k-points mesh according to a Monkhorst-Pack scheme. Geometrical optimization

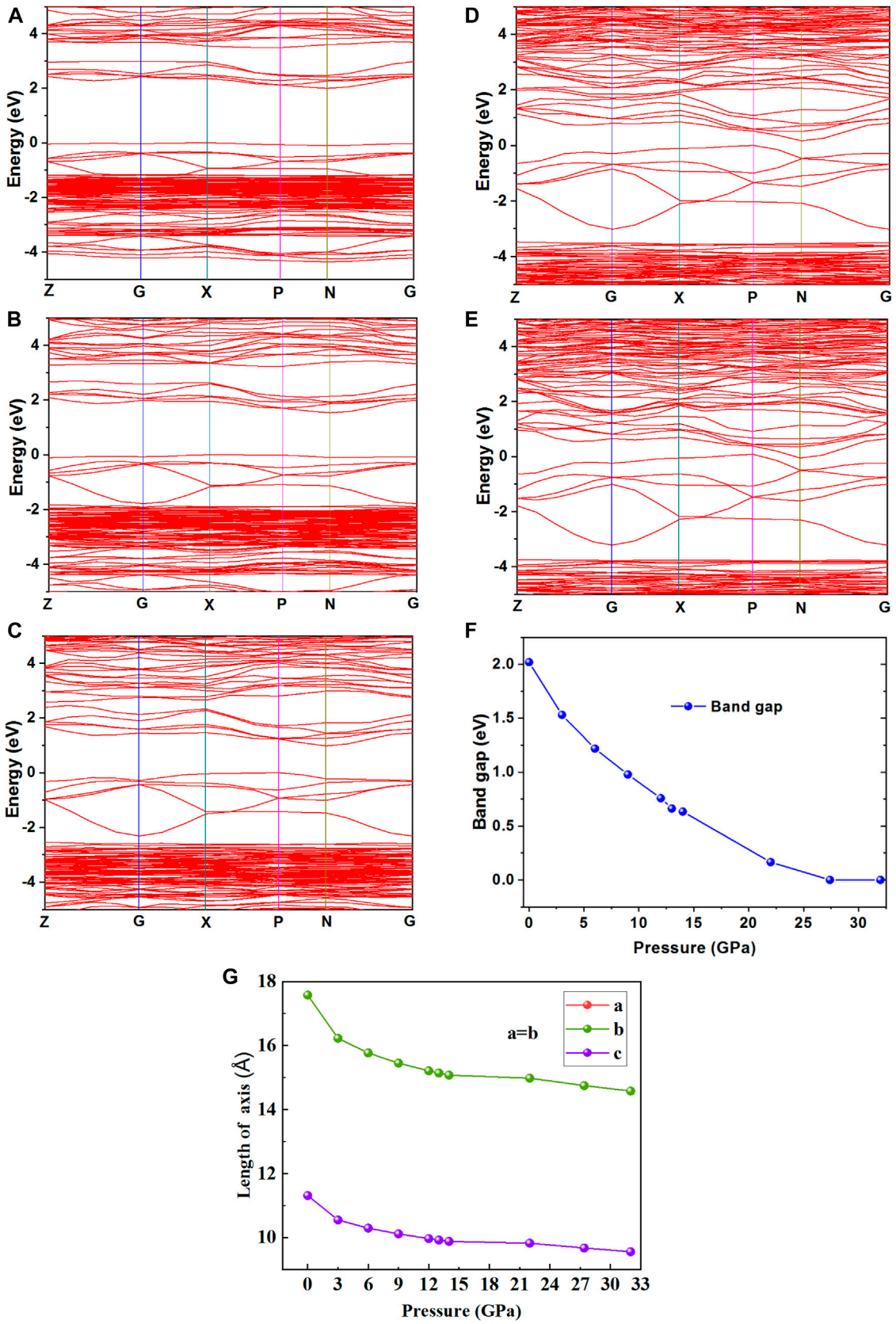

FIGURE 2 | (Color online) Band structure and lattice constants at different pressure for Cs_2In**(I)**In(III)Cl_6 **(A)** 0 GPa, **(B)** 3 GPa **(C)** 9 GPa, **(D)** 22 GPa **(E)** 32 GPa, **(F)** variation of band gaps at different pressures, and **(G)** variation of lattice constants at different pressures.

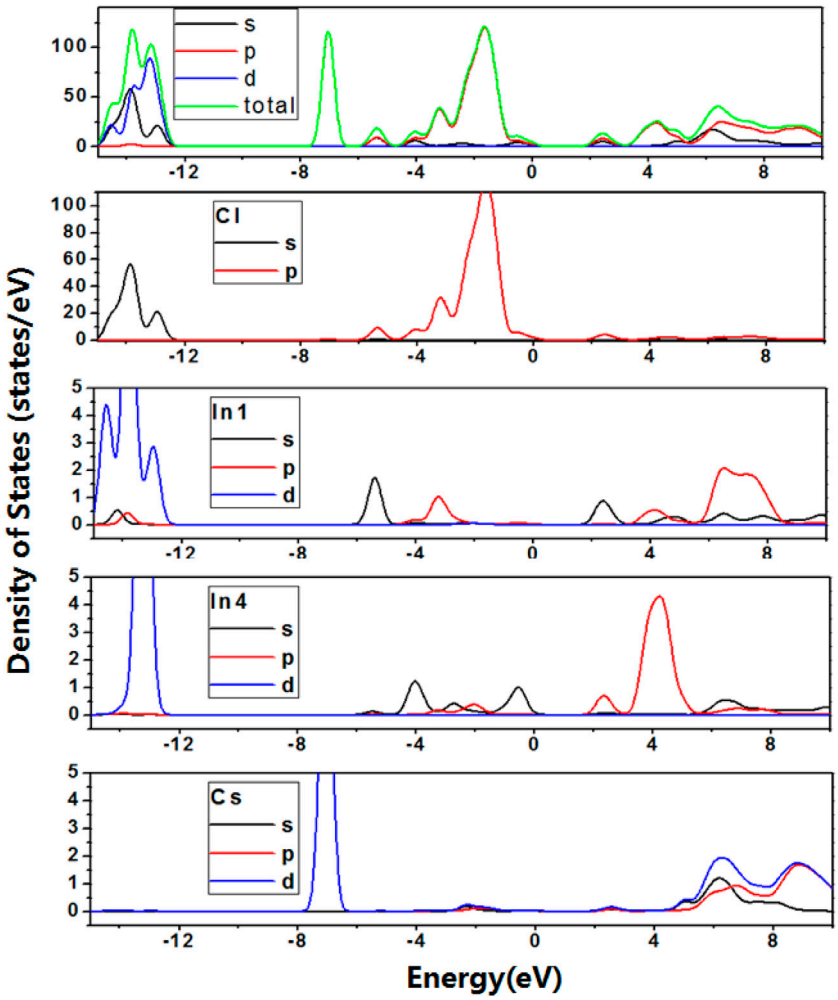

FIGURE 3 | (Color online) Density of states and Partial density of states for $Cs_2In(I)In(III)Cl_6$ at 0 GPa pressure. The data for *y*-axis indicates the density of States (electrons/eV), and the data for *x*-axis indicates the photon energy (eV).

was conducted using the convergence of thresholds of 5×10^{-6} eV/atom for the total energy, all forces on atoms were converged to less than 0.01 eV/Å. The crystal structures have been energy-optimized by the above calculation method.

The linear optical properties for $Cs_2In(I)In(III)Cl_6$ can be obtained from the frequency-dependent complex dielectric function $\varepsilon(\omega) = \varepsilon_1(\omega) + i\varepsilon_2(\omega)$, where $\varepsilon_1(\omega)$ and $\varepsilon_2(\omega)$ are the real and imaginary parts of the dielectric function, and ω is the photon frequency. The frequency-dependent linear optical spectra, e.g., refractive index $n(\omega)$, extinction coefficient $\kappa(\omega)$, absorption coefficient $\alpha(\omega)$, energy-loss function $L(\omega)$, and reflectivity $R(\omega)$ can be calculated from the real part $\varepsilon_1(\omega)$ and the imaginary part $\varepsilon_2(\omega)$). Refractive index is formulated as

$$n(\omega) = \left(\frac{\varepsilon_1(\omega) + \sqrt{\varepsilon_1^2(\omega) + \varepsilon_2^2(\omega)}}{2} \right)^{\frac{1}{2}}, \quad (1)$$

Similarly, extinction coefficient is denoted by $\kappa(\omega)$ and is calculated as

$$\kappa(\omega) = \left(\frac{-\varepsilon_1(\omega) + \sqrt{\varepsilon_1^2(\omega) + \varepsilon_2^2(\omega)}}{2} \right)^{\frac{1}{2}}. \quad (2)$$

General formula of reflectivity to find the reflection from surface of any material is given as

$$R(\omega) = \frac{(n-1)^2 + \kappa^2}{(n+1)^2 + \kappa^2}. \quad (3)$$

In the same way, absorption coefficient $\alpha(\omega)$ has been determined by using the following relation:

$$\alpha(\omega) = 4\pi\kappa(\omega)/\lambda, \quad (4)$$

RESULTS AND DISCUSSIONS

The calculations were conducted on the $Cs_2In(I)In(III)Cl_6$ version of the structural model as shown in **Figure 1**, that is,

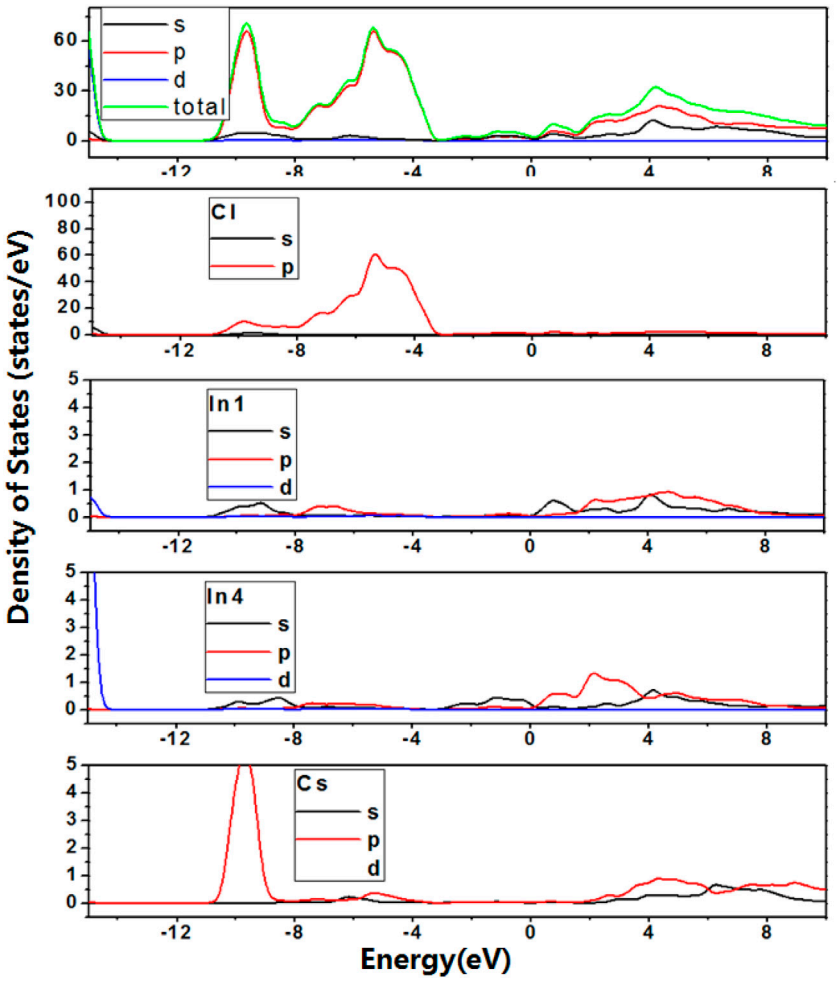

FIGURE 4 | (Color online) Density of states and Partial density of states for $Cs_2In(I)In(III)Cl_6$ at 27.5 GPa pressure. The data for *y*-axis indicates the density of States (electrons/eV), and the data for *x*-axis indicates the photon energy (eV).

without considering the apparent presence of Cs in the In sites or attendant vacancies in the crystal structure of $Cs_2In(I)In(III)Cl_6$. The crystallographic data of $Cs_2In(I)In(III)Cl_6$, according to the structural model described in **Table 1**. The structure of the $Cs_2In(I)In(III)Cl_6$ sample is very similar to that of $CsTlCl_3$ (Retuerto et al., 2013). In this structure, there are two Cs sites, four In sites, and seven Cl sites. In1, In2, and In3 are octahedrally coordinated, whereas In4 is at the center of a pentagonal bipyramid. The charge of In on In1 and In2 sites can be assigned to 3^+. The remaining two nominal In sites indicate a lower oxidation state on In3 and In4 sites. One would conclude that In^+ occupies In3 and In4 sites.

Figure 2 represents electronic band structures of $Cs_2In(I)In(III)Cl_6$ under different pressures. It has been observed that under ambient conditions, the top of the valence band (VB) and bottom of the conduction band (CB) are located at X and N symmetry points, respectively, and the band-gap Eg calculated under ambient pressure is 2.02 eV (**Figure 2A**). Hence, $Cs_2In(I)In(III)Cl_6$ is regarded as an indirect band-gap semiconductor. Interestingly, while increasing the pressure, shifting the top of VB at P symmetry points toward the Fermi level was observed. Contrary to this, other symmetry points were observed to move away from the Fermi level. With the increasing pressure, the band-gap decreases and becomes zero at ~27.5 GP, as shown in **Figure 2F**, which indicates the semiconductor-metal transition with the increasing pressures. The lattice constant *a* ($a = b$) ranges from 17.5779 Å (ambient pressure) to 14.5797 Å (32 GPa), and c ranges from 11.3175 to 9.5625 Å (**Figure 2G**). It is well known that GGA functional underestimates in calculating the electronic band-gap, but the use of hybrid exchange-correlation functionals, such as HSE06 and mBJ, provides better results (Tan et al., 2019). In addition, the calculated band gap here is much larger than the literature report (<1 eV) of theoretical $CsInCl_3$ (Körbel et al., 2016). This is possibly attributed to the calculations carried out based on the experimental crystal structure. Meanwhile, we observe the semiconductor-metal transition appears at ~27.5 GPa in our theoretical result, which is larger than experimental result (~22 GPa) (Lin et al., 2019a). This could be attributed to the removal of some disorder components in our model, compared with the crystal structure shown in the

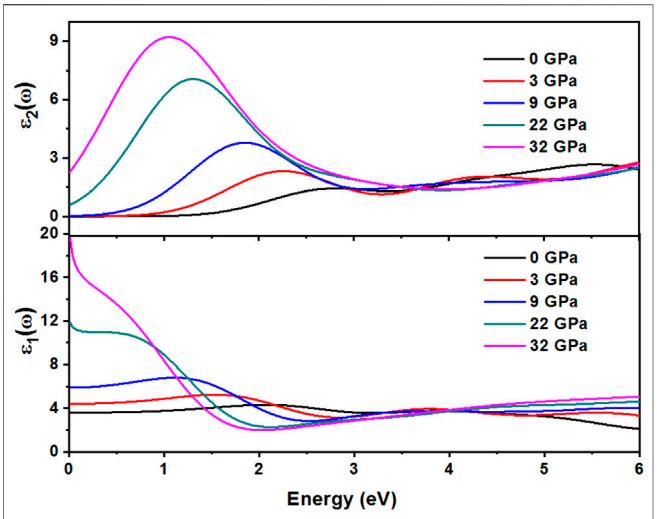

FIGURE 5 | (Color online) Dielectric function of $Cs_2In(I)In(III)Cl_6$ at different pressures.

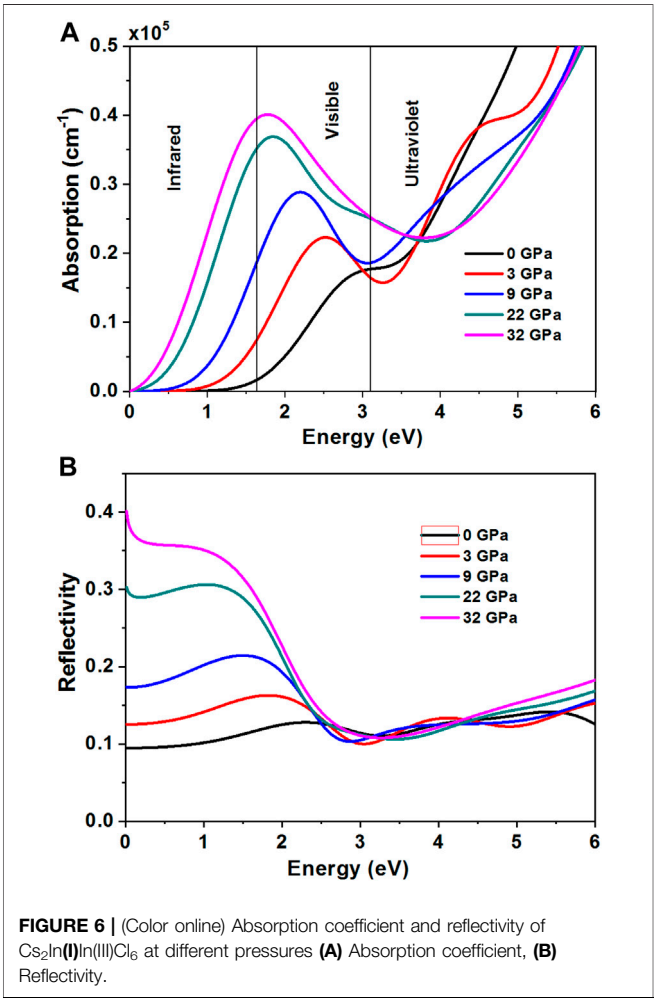

FIGURE 6 | (Color online) Absorption coefficient and reflectivity of Cs_2In**(I)**$In(III)Cl_6$ at different pressures **(A)** Absorption coefficient, **(B)** Reflectivity.

Reference Lin et al. (2019a). The large indirect band gap suggests that this nonstoichiometric perovskite-derived phase is not a good candidate for photovoltaic application. These theoretical and experimental results, however, provide a basis for designing related inorganic halide perovskites for potential photovoltaic functions or superconductivity.

To further reveal the factors controlling the bandgap trends, density of states (DOS) and partial density of states (PDOS) based on variable control approaches were carried out. Firstly, to study the effect of In cations on bandgap trend, DOS and PDOS of $Cs_2In(I)In(III)Cl_6$ were calculated at 0 GPa, and shown in **Figure 3**. The calculation results indicated that In on In2 and In3 sites do not contribute to the basic electronic structures. The valence band maximum (VBM) is derived from the p orbitals of In on In4 sites and p orbitals of Cl, and their overlapping indicates the significant hybridization. The s orbitals of In on In1 sites, p orbitals of In on In4 sites and p orbitals of Cl constitute the conduction band minimum (CBM). The trend of difference value between VBM and CBM for $Cs_2In(I)In(III)Cl_6$ is consistent with the change of calculated bandgaps. With the increase in pressure from 0 to 27.5 GPa, the s and p orbitals of In on In1 sites, and the s and p orbitals of In on In4 sites lowered the bottom of conduction band (see **Figure 4**), and the metal–insulator transition occurs in the $Cs_2In(I)In(III)Cl_6$.

The real and imaginary parts of dielectric function for $Cs_2In(I)In(III)Cl_6$are shown in **Figure 5**. The complex dielectric function$\varepsilon(\omega) = \varepsilon_1(\omega) + i\varepsilon_2(\omega)$completely describes the optical properties of a medium for different photon energies. The peak value of real part of the dielectric constant is related to the electron excitation. The real part can be derived from the imaginary part $\varepsilon_2(\omega)$by the Kramers–Kronig relation. With an increase in pressure from 0 to 32 GPa, the peak value of the real part $\varepsilon_1(\omega)$ of the dielectric function increases in visible and infrared regions, while imaginary dielectric function decreases.

The absorption coefficient determines the solar energy conversion efficiency and it indicates how far light of a specific energy (frequency) can penetrate into the material before absorption. With increasing pressure, the peak value of the absorption coefficient increases in visible and infrared regions as shown in **Figure 6A**. The electron excitation produces the red-shift of the peak value of the optical absorption coefficient. The reflectivity spectrum as a function of photon energy is shown in **Figure 6B**. We have observed that the reflectivity decreases with increasing pressure in visible and infrared regions.

CONCLUSION

In conclusion, using the first principle method, we studied theoretically and in detail the structural, optical, and electronic properties of a charge-ordered indium halide perovskite $Cs_2In(I)In(III)Cl_6$ at high pressure, based on the experimental crystal structure. With increasing pressure, the band gap of $Cs_2In(I)In(III)Cl_6$ decreases, which shows a semiconductor-to-metal phase transition under high pressures 27.5 GPa. The theoretical result is larger than the experimental result

(~22 GPa) due to the removal of disorder in the model. The peak value of optical absorption coefficient produces red-shift, and the reflectivity decreases in visible and infrared regions with increasing pressure. Meanwhile, the results show that high-pressure research provides a powerful tool to tune structures and properties. Thus, the properties of materials could be better understood by the method.

DATA AVAILABILITY STATEMENT

The raw data supporting the conclusions of this article will be made available by the authors, without undue reservation.

AUTHOR CONTRIBUTIONS

LP proposed the research idea and analysis; YW and SY performed theoretical calculations and manuscript; All authors reviewed the manuscript, have given approval to the final version of the manuscript, and confirmed the authorship to this work.

FUNDING

This work is sponsored by the National Natural Science Foundation of China (61875119), Shanghai Rising-Star Program (Grant No. 19QA1404000) and the Natural Science Foundation of Shanghai (No. 17ZR1411400).

REFERENCES

Amgar, D., Aharon, S., and Etgar, L. (2016). Inorganic and hybrid organo-metal perovskite nanostructures: synthesis, properties, and applications. *Adv. Funct. Mater.* 26, 8576–8593. doi:10.1002/adfm.201603752

Chen, S., Zhang, T., Liu, X., Qiao, J., Peng, L., Wang, J., et al. (2020). Lattice reconstruction of La-incorporated CsPbI2 Br with suppressed phase transition for air-processed all-inorganic perovskite solar cells. *J. Mater. Chem.* 8, 3351–3358. doi:10.1039/c9tc05736f

Dreizler, R. M., and Gross, E. K. U. (1990). *Density functional theory*. Heidelberg: Springer.

Filip, M. R., Eperon, G. E., Snaith, H. J., and Giustino, F. (2014). Steric engineering of metal-halide perovskites with tunable optical band gaps. *Nat. Commun.* 5, 5757. doi:10.1038/ncomms6757

Han, J. S., Le, Q. V., Choi, J., Hong, K., Moon, C. W., Kim, T. L., et al. (2018). Lead-free all-inorganic cesium tin iodide perovskite for filamentary and interface-type resistive switching toward environment-friendly and temperature-tolerant nonvolatile memories. *ACS Appl. Mater. Interf.* 28, 1705783. doi:10.1002/adfm.201705783

He, X., Liu, P., Zhang, H., Liao, Q., and Yao, J. (2017). Patterning multicolored microdisk laser arrays of cesium lead halide perovskite. *Adv. Mater.* 29, 1604510. doi:10.1002/adma.201604510

Jeong, B., Han, H., Choi, Y. J., Cho, S. H., Kim, E. H., Lee, S. W., et al. (2018). Polymer-assisted nanoimprinting for environment-and phase-stable perovskite nanopatterns. *Adv. Funct. Mater.* 28, 1706401. doi:10.1002/adfm.201706401

Körbel, S., Marques, M. A. L., and Botti, S. J. (2016). Stability and electronic properties of new inorganic perovskites from high-throughput ab initio calculations. *J. Mater. Chem. C* 4, 3157–3167. doi:10.1039/c5tc04172d

Kovalenko, M. V., Protesescu, L., and Bodnarchuk, M. I. (2017). Properties and potential optoelectronic applications of lead halide perovskite nanocrystals. *Science* 358, 745–750. doi:10.1126/science.aam7093

Li, M., Liu, T., Wang, Y., Yang, W., and Lü, X., (2020). Pressure responses of halide perovskites with various compositions, dimensionalities, and morphologies. *Matter Radiat. Extremes* 5, 018201. doi:10.1063/1.5133653

Lin, J., Chen, H., Gao, Y., and Cai, Y. (2019a). ,Pressure-induced semiconductor-to-metal phase transition of a charge-ordered indium halide perovskite. *Proc. Natl. Acad. Sci.* 116 (47), 23404–23409. doi:10.1073/pnas.1907576116

Lin, J., Chen, H., and Kang, J. (2019b). Copper (I)-based highly emissive all-inorganic rare-earth halide clusters. *Matter* 1, 180–191. doi:10.1016/j.matt.2019.05.027

Lin, J., Lai, M., and Dou, L. (2018). Thermochromic halide perovskite solar cells. *Nat. Mater.* 17, 261–267. doi:10.1038/s41563-017-0006-0

Retuerto, M., Emge, T., Hadermann, J., Stephens, P. W., and Li, M. R. (2013). Synthesis and properties of charge-ordered thallium halide perovskites, CsTl+ 0.5 Tl3+ 0.5 X3 (X= F or Cl): theoretical precursors for superconductivity? *Chem. Mater.* 25, 4071–4079. doi:10.1021/cm402423x

Tan, X., Stephens, P., and Hendrickx, M. (2019). Tetragonal Cs1. 17In0. 81Cl3: a charge-ordered indium halide perovskite derivative. *Chem. Mater.* 31, 1981–1989. doi:10.1021/acs.chemmater.8b04771

Vargas, B., Ramos, E., Perez-Gutierrez, E., Alonso, J. C., and Solis-Ibarra, D. J. (2017). A direct bandgap copper–antimony halide perovskite. *J. Am. Chem. Soc.* 139, 9116–9119. doi:10.1021/jacs.7b04119

Volonakis, G., Haghighirad, A. A., Milot, R. L., Sio, W. H., Filip, M. R., Wenger, B., et al. (2017). Cs2InAgCl6: a new lead-free halide double perovskite with direct band gap. *J. Phys. Chem. Lett.* 8, 772–778. doi:10.1021/acs.jpclett.6b02682

Yin, Z. P., and Kotliar, G. (2013). Rational material design of mixed-valent high-Tc superconductors. *Europhys. Lett.* 101, 27002. doi:10.1209/0295-5075/101/27002

Zhao, X., Yang, J., Fu, Y., Yang, D., Xu, Q., Yu, L., et al. (2017). Design of lead-free inorganic halide perovskites for solar cells via cation-transmutation. *J. Am. Chem. Soc.* 139, 2630–2638. doi:10.1021/jacs.6b09645

Conflict of Interest: The authors declare that the research was conducted in the absence of any commercial or financial relationships that could be construed as a potential conflict of interest.